Published in final edited form as:
*Nanotechnology*. 2010 April 30; 21(17): 175704. doi:10.1088/0957-4484/21/17/175704.

# Preparation and Characterization of a Magnetic and Optical Dual-Modality Molecular Probe

**A Bumb**[1], **C A S Regino**[2], **M R Perkins**[3,5], **M Bernardo**[4], **M Ogawa**[2], **L Fugger**[5], **P L Choyke**[2], **P J Dobson**[6], and **M W Brechbiel**[1]

[1]Radioimmune & Inorganic Chemistry Section, Radiation Oncology Branch, NCI, NIH, Building 10, Room 1B53, 10 Center Drive, Bethesda, MD 20892, USA. Bumba@mail.nih.gov, martinwb@mail.nih.gov

[2]Molecular Imaging Program, NCI, NIH, Building 10, Room B3B69, 10 Center Drive, Bethesda, MD 20892, USA.

[3]Vaccine Research Center, NIAID, NIH, Building 40, Room 3608B, 40 Convent Drive, Bethesda, MD 20892, USA.

[4]SAIC-Frederick Inc., NCI-Frederick, Frederick, MD 21702, USA.

[5]MRC Human Immunology Unit, Weatherall Institute of Molecular Medicine, John Radcliffe Hospital, The University of Oxford, Oxford OX3 9DS, UK.

[6]Oxford University Begbroke Science Park, Sandy Lane, Kidlington, Oxon OX5 1PF, UK.

## Abstract

Multi-modality imaging probes combine the advantages of individual imaging techniques to yield highly detailed anatomic and molecular information in living organisms. Herein, we report the synthesis and characterization of a dual-modality nanoprobe that couples the magnetic properties of ultrasmall superparamagnetic iron oxide nanoparticles (USPIOs) with the near infrared fluorescence of Cy5.5. The fluorophore is encapsulated in a biocompatible shell of silica surrounding the iron oxide core for a final diameter of ~17 nm. This silica-coated iron oxide nanoparticle (SCION) has been analyzed by transmission electron microscopy, dynamic light scattering, and superconducting quantum interference device (SQUID). The particle demonstrates a strong negative surface charge and maintains colloidal stability in the physiological pH range. Magnetic hysteresis analysis confirms superparamagnetic properties that could be manipulated for thermotherapy. The viability of primary human monocytes, T cells, and B cells incubated with particle has been examined *in vitro*. *In vivo* analysis of agent leakage into subcutaneous A431 tumors in mice was also conducted. This particle has been designed for diagnostic application with magnetic resonance and fluorescence imaging, and has future potential to serve as a heat-sensitive targeted drug delivery platform.

## 1. Introduction

Nanoparticle technology has attracted immense interest in the past two decades for bioimaging and biosensing research because of its capability to obtain sensitive data in a noninvasive manner. However, effective application of this technology relies greatly on robust nanoparticle engineering and synthesis techniques. The development involves design, synthesis, surface modification and extensive characterization. The performance of a nanoprobe relies greatly on factors such as particle composition, size, surface charge, surface functionality, biocompatibility, contrast sensitivity, and stability [1]. Analyzing the

agent's water dispersion under physiological conditions (i.e. pH 7.4) is a first step to understanding how successful it will be as a "nano"-tool.

Ultrasmall superparamagnetic iron oxide nanoparticles (USPIOs) are proving to be a class of agents useful for *in vitro* and *in vivo* cellular and molecular imaging. Maghemite/magnetite, $\gamma$-$Fe_2O_3$/$Fe_3O_4$, particles have face-centered cubic packing of oxygen that allows electrons to jump between iron ions occupying interstitial tetrahedral and octahedral sites. This gives the molecules half-metallic properties that greatly shorten transverse relaxation times, $T_2$ and $T_2$*, and can increase proton relaxivities ten-fold [1]. USPIOs typically are comprised of iron crystals of 5–12 nm and exhibit prolonged blood half-life that affords them the opportunity to eventually cross capillary walls and have more widespread tissue distribution. They can be delivered to the interstitium by non-specific vesicular transport and through transendothelial channels. Once in the interstitium, draining lymphatic vessels transport them to lymph nodes, thus making them suitable agents for MR lymphography (MRL). At low concentrations, these agents can be used for $T_1$-weighted magnetic resonance angiography (MRA), though high concentrations will lead to signal loss due to $T_2$-shortening effects. Unlike many nanoprobes, iron-based nanoparticles have a well recognized metabolic fate *in vivo* that has been accepted by regulatory agencies.

The goal of designing molecular imaging probes is to make particles that are targetable and imageable. Multimodal particles can provide advantages that traditional single modality agents lack. While MRI is a non-invasive technique that has exquisite resolution, its sensitivity is lower than radioactive and optical methods. Optical imaging has greater sensitivity and the potential for real-time imaging, but with limited depth perception. Thus, an agent that provides signal in both imaging domains could be a useful diagnostic tool. Furthermore, for *in vitro* studies, fluorescent nanoparticles provide compatibility with confocal microscopy and flow cytometry, whereas the magnetic properties would allow for ease of separation by use of a strong magnet in techniques such as magnetic activated cell sorting (MACS).

A continuation from the work published in this journal in 2008 [2], herein we describe the synthesis and characterization of a dual-modality nanoparticle that combines the magnetic properties of USPIOs with the fluorescence properties of the near infrared (NIR) fluorophore Cy5.5, a cyanine dye with excitation and emission peaks at 675 nm and 694 nm, respectively. With an absorption coefficient of tissue that is considerably smaller in the NIR region (~700 to 900 nm), light can penetrate more deeply into tissue to depths of several centimeters albeit with considerable diffusion [3,4]. Additionally, NIR fluorophores, such as Cy5.5, minimize signal contamination from autofluorescence arising from intrinsic biomolecules typically occuring in the visible light spectrum, 350–700 nm [5,6]. Cy5.5 has superior photostability compared to more commonly used dyes, such as fluorescein, and has a high extinction coefficient ($\varepsilon$ = 190000 $M^{-1}cm^{-1}$ in PBS) [7]. Cy5.5 is a standard dye used for NIR imaging that permits those familiar with optical imaging to have a standard for comparative purposes, however the chemistry described in the following text is interchangeable with other dyes amenable to this same conjugation chemistry. Because the dye is encapsulated within the silica, particle properties are expected to remain very similar, if not the same.

To be used *in vivo*, it is necessary to functionalize USPIOs with a surface coating, such as silica, that provides stability and enhances biocompatibility. Silica plays a role in maintaining stability for particle suspensions during changes in pH or electrolyte concentration due to silanol groups that make the surface lyophilic [8]. Additionally, it is well known for optical transparency [9], enabling excitation and emission light to pass through the silica matrix efficiently. Silica encapsulation may also enhance photostability by

providing a protective layer around encapsulated optical agents [10,11]. Specifically here, Cy5.5 is highly lipophilic, which is what often contributes to its uptake and metabolism in the liver. Its encapsulation could improve biodistribution and prevent its release from the particle, while improving the stability of the dye itself. Silica is dispersible in aqueous and non-aqueous solutions and its size characteristics are unaffected by changes in solvent polarity, making it resistant to swelling. It is resistant to microbial attack, while appearing to be non-toxic and biocompatible [12,13]. Highly pertinent to nanoprobe development, silica deposition can be controlled for a tunable layer thickness. Finally, the surface of silica is coated with silanol groups that easily react with alcohols and silane coupling agents [14] for strong covalent bonding with ligands, such as proteins, peptides, sugars, antibodies and oligonucleotides.

Utilizing these properties of silica, USPIOs, and NIR fluorophores, a silica-coated iron oxide nanoparticle (SCION) has been synthesized and characterized. The goal of this work was not only to develop a dual-modal agent, but also to encapsulate the dye in a biocompatible shell and keep the particle small in size relative to other iron oxide agents to have a more desirable clearance profile for further work with targeting. Moreover, while small dual-modality agents can be developed off dendrimer structures, the superparamagnetism of USPIOs allows that in addition to diagnostics, the particles can be used in therapeutic applications.

## 2. Experimental

### 2.1. USPIO synthesis and initial silica encapsulation

As described in Bumb et al [2], the co-precipitation of ferrous and ferric salts in alkaline and acidic aqueous phase was used to prepare colloids of $Fe_3O_4$ nanoparticles with a diameter of ~9 nm. To functionalize the magnetic particles for *in vivo* application while maintaining a small diameter to prevent clearance, the surface was coated with a 2 nm layer of silica. The mechanism of silica deposition was hydrolysis of an alkoxy silane followed by condensation of alcohol and water [15]:

$$\equiv Si - OR + H_2O \leftrightarrow \equiv Si - OH + ROH \quad (1)$$

$$\equiv Si - OR + \equiv Si - OH \leftrightarrow \equiv Si - O - Si \equiv + ROH \quad (2)$$

$$\equiv Si - OH + \equiv Si - OH \leftrightarrow \equiv Si - O - Si \equiv + H_2O \quad (3)$$

To ensure even distribution and prevent aggregation, 30 nmol USPIO was intially sonicated in 2.5 mL deionized (DI) water for 10 min before adding 2.5 mL of 10% v/v tetraethylorthosilicate (TEOS) in ethanol. To catalyze the reaction, 100 μL of triethylamine (TEA) were added. The reaction was run under sonication for 15 min and then washed mulitple times by magnetic separation with DI water.

### 2.2. Cy5.5-APTES Conjugation and Characterization

Fluorophore Cy5.5 was purchased from GE Healthcare with an *N*-hydroxysuccinimide (NHS) ester group. Cy5.5 and 3-aminopropyltriethoxysilane (APTES) were reacted in methanol for 4 h in room temperature at a molar ratio of 1.3:1.

Thin layer chromatography (TLC) was used to confirm conjugation in the APTES-Cy5.5 sample. A silica plate was spotted with the two starting agents and the product and then placed in a reservoir of 20% v/v methanol in chloroform. The separated spots were visualized with ultraviolet light and by iodine vapor. Quantitative analysis was performed by comparing retardation factors, $R_f = d_{sample}/d_{solvent}$, where $d$ was the distance from the start line to the center of the spot.

Reverse-phase HPLC and offline mass spectrometry were also used to confirm the reaction. Reverse-phase HPLC was performed using two Gilson Model 303 pumps, a Gilson 803C manometric module, a Gilson 811B dynamic mixer, and a Knauer ultraviolet detector all connected through a Gilson 506C system interface module and operated by UniPoint version 1.65 software. Purification was achieved with a Hamilton Prp-1 polymer reversed-phase semi-preparative column (10 μm, 7.0 mm × 30.5 cm) using binary solvent system (A = 0.15 M $NH_4OAc$ pH 6.5, B = MeOH) at a linear gradient (50% B over 30 min) with a flow rate of 3 mL/min. Fractions were collected from the separation and analyzed for product.

Mass spectra were obtained on a Waters LCT Premier Time-of-Flight Mass Spectrometer using electrospray ionization (ESI/TOF/MS) operated in the negative ion mode. The electrospray capillary voltage was 3 kV, and the sample cone voltage was 60 V. The desolvation temperature was 225 °C, and the desolvation gas flow rate of nitrogen was at 300 L/h. Accurate mass determinations were obtained using the internal standard method and processed with the MassLynx 4.0 software.

### 2.3. Dye attachment to particle core and final silica encapsulation

The free alkoxy silane groups of the Cy5.5-APTES conjugate were left to attach to the particle surface by the previously described mechanism. The silylated dye was incubated for 48 h with the particle core at an equivalence of 20 dye molecules per particle and then washed by magnetic separation multiple times with DI water. Initially, Cy5.5 was conjugated directly to the surface of USPIO. In this case, though the color of the particles to the naked eye visibly changed with conjugation of the dye, no fluorescence activity was found when examined in a Perkin Elmer LS55 fluorescence spectrophotometer (figure 1). This occurance may be due to absorption by the USPIO. Iron oxide nanocrystals have been shown to possess a broad absorption spectrum from 400 to 600 nm [16]. Thus, USPIOs were first coated with silica and then conjugated to Cy5.5. With the initial silica coating, the particles did fluoresce at the expected wavelength (figure 1). Therefore, the thin silica layer provided a “buffer layer” to protect the dye activity.

The Cy5.5-silica-USPIO particles were then coated with a final layer of silica to encapsulate the dye and make the outer surface of the particle biocompatible. The additional layer of silica was applied using the same protocol described above when coating UPSIO with silica. However, triethylamine was not used to catalyze the reaction, as it could increase basic conditions and damage dye structure. The synthesis of the complete dual-imageable silica-coated iron oxide nanoparticle (SCION) is shown in figure 2. Iron content was analyzed by inductively coupled plasma optical emission spectrometry (Colombia Analytical Services, Tucson, Arizona) and yielded 4.46 mmol Fe/g SCION.

### 2.4. SCION Particle Characterization

SCION size was characterized by three methods. Using transmission electron microscopy, the particle diameter and silica layer thickness were analyzed during each step of synthesis. Multiple samples were drop-cast onto carbon grids and images were collected with a JEOL4000EX microscope. Gatan Digital Micrograph 3.6.1 software was used to measure

size, where a particle's diameter was determined as the mean of three cross-sectional measurements.

SCION solution iron and silica percent mass were analyzed in duplicate by inductively coupled plasma optical emission spectrometry (Desert Analytics, Tucson, Arizona) and used to calculate silica layer thickness with the assumptions that solution density was equal to that of water and silica was deposited evenly to form spherical particles.

Using a Malvern Zetasizer Nano ZS, the hydrodynamic diameter by number distribution and zeta potential of the SCION particles were evaluated. Adjustments in pH were made with potassium hydroxide and hydrochloric acid.

To characterize the particle's magnetic behavior, magnetic hysteresis curves were determined with a superconducting quantum interference device (Quantum Design MPMS XL). The temperature was held constant at 310 K (body temperature) for susceptibility measurements in two applied field ranges: ±7 T and ±0.01 T.

Though Cy5.5's peak excitation is at 675 nm, during cell studies with flow cytometry excitation would be at 635 nm. Thus, the fluorescence of SCION with a 635 nm excitation was checked using Perkin Elmer LS55 fluorescence spectrophotometer.

### 2.5. Cell Viability

*In vitro* studies with flow cytometry were conducted on peripheral blood mononuclear cells (PBMCs) that were obtained from healthy volunteers participating in the NIH research apheresis program. PBMCs were chosen because they are primary human cells and represent a range of cell types that could potentially interact with particles that would be injected intravenously. Cells were isolated by standard Ficoll-Hypaque (GE Healthcare) density gradient centrifugation and kept in RPMI 1640 media supplemented with 10% heat-inactivated fetal calf serum, 100 U/mL penicillin, 100 μg/ml streptomycin, and 2 mM L-glutamine.

Two viability studies were conducted. In the first, PBMCs (10 million cells/mL in media) were incubated for 1 h at 37°C with SCION at a concentration of 0.05 nmol/mL (staining optimized from a titration of 0 – 0.1 nmol/mL SCION). They were then washed, resuspended in media (1 million cells/mL) and analyzed with flow cytometry at 0, 1, 2, 4, 8, 24, 48, and 72 h post-incubation. A control of the same cells that were not incubated with particle was drawn from for each time point. In the second study, cells ($10^6$ cells/mL in media) were incubated with SCION (0.05 nmol/mL) for 0, 1, 4, 8, 24, or 48 h. To standardize for PBMC viability over time *in vitro*, the incubations were performed in reverse order and all samples analyzed by flow cytometry together at the end so that all the cells remained in culture for the same amount of time. In other words, the 48 h-incubation sample was started first, 24 h-incubation sample 24 h later, 8 h-incubation sample 16 h after that, and so on. Thus, the control for all samples was the sample that remained unstained during the incubation period (0 h). Time points up to 24 h in both studies were conducted on PBMCs obtained from two volunteers and the remaining time-points on cells from one.

For flow analysis, all samples were stained with aqua amine reactive viability dye (Invitrogen) and cell population markers αCD3 Cy7PE (clone SK7, Becton Dickinson), αCD19 PE (clone HIB19, Becton Dickinson), and αCD14 PacificBlue (clone M5E2, Becton Dickinson Pharmingen, conjugated in-house at the NIH VRC in accordance with standard protocols available at: http://drmr.com/abcon/index.html). The cells were then fixed in 1% paraformaldehyde in PBS. For each sample, between 200,000 and $10^6$ events were acquired on an LSR II flow cytometer (BD Biosciences, San Jose, CA) and analyzed with FlowJo

software (Tree Star, Inc.). Singlet cells were gated to separate CD3+ T cells, CD19+ B cells, and CD14+ monocytes before each cell populations was analyzed for viability and SCION staining.

### 2.6. Animal Studies

SCION particle was examined for enhanced permeability and retention (EPR) effect in tumor-bearing mice. All procedures were carried out in compliance with the Guide for the Care and Use of Laboratory Animal Resources (1996), National Research Council, and approved by the NIH Animal Care and Use Committee. Human epithelial carcinoma A431 cells ($2 \times 10^6$) were injected s.c. in the left hind leg of female athymic (*nu/nu*) mice (Charles River Laboratories, 4–6 weeks old). The experiments were performed 14 to 18 d after cell injection.

Intravenous injections of SCION (50 μL of 45mM Fe SCION in saline) were given to mice (n=4) bearing A431 tumors. MR images were obtained prior to injection of the imaging agent and post-injection at 1, 2, 4, and 22 h using a 3T clinical scanner (Achieva, Philips Medical Systems) equipped with a saddle-shaped receive only coil with an inner diameter of 32 mm and a coil length of 77 mm. Multiple-echo gradient echo images (repetition time of 94.1 ms, echo times of 4.60, 8.05, 11.50, 14.95 ms, 24° flip angle, voxel size of 0.16 × 0.16 × 0.30 mm, resolution of 6.400 pixels per mm). Particle retention was examined by analyzing $R_2$* maps using an in-house built IDL software.

## 3. Results and Disussion

### 3.1. Chromatography Characterization of Cy5.5-APTES

$R_f$ values of Cy5.5, APTES-Cy5.5, and APTES were 0.36, 0.49, and 0.03, respectively. The dye conjugate traveled 38% further on the polar silica plate than the more polar Cy5.5 (-NHS ester), confirming conjugation.

### 3.2. Identification of APTES-Cy5.5 Product

Cy5.5 dye conjugation to APTES prior to linakge with the nanoparticle was monitored by RP-HPLC and confirmed by MS. In this case, a sample conjugation solution was injected to the RP-HPLC and fractions collected to identify the peaks and product. The major peak found at 18 min retention time identified it as the dehydrated form of the product Cy5.5-APTES. TOF/MS/ES (−): Calculated *m/z* for $[C_{88}H_{98}N_6O_{30}S_8Si_2]^{4-}$: 507.5925; Found: 507.5803. Calculated *m/z* for $[C_{88}H_{1008}N_6O_{30}S_8Si_2]^{2-}$: 1016.195; Found: 1016.1942. This dehydrated form of the product was not unexpected as in dehydration and desolvation is normal in acquiring *m/z* ions in MS and in the electrospray mode.

### 3.3. SCION Size and Surface Charge Characterization

Iron oxide is readily visualized by TEM (figure 3) and the particle size can be estimated at known magnifications. Note, however, the technique may potentially underestimate particle size because the edges of these crystals are difficult to define accurately since the boundaries are thinner than the centers and densely-packed opaque areas can also hamper analysis by obscuring individual particles. With the assumption that the particles are spherical, USPIO diameter had a lognormal distribution, as is typical with such crystals [17], where the geometric mean diameter was 9.2 nm (std dev = 1.1 nm). Silica layer thickness after initial silica deposition, dye conjugation, and then final silica encapsulation was 2.6 nm (std dev = 0.56 nm), 2.7 nm (std dev = 0.35 nm), and 3.6 nm (std dev = 0.47 nm), respectively. A one-tail t-test comparing silica thickness pre- and post-dye dye conjugation was statistically insignificant with a p-value of 0.289, confirming that Cy5.5 attachment did not degrade the

silica layer. The same t-test comparing final particle silica layer thickness to synthesis steps pre- and post-dye conjugation was significant at p = 3.27e-6 and p = 5.88e-7, respectively.

Final layer thickness was also evaluated using elemental analysis of Si content. SCION sample mass was composed of 30.1% iron and 29.0% silicon. Calculations made with a magnetite core diameter of 9.2 nm revealed a silica layer of ~1.2 nm, a value less than that obtained by TEM. This difference exists for number of reasons. The density values used for the above calculations are based on dry density. However, silica is well known for its water absorbing properties and is a commonly used desiccant. Hydrated and dry silica have different properties, including density. Furthermore, in TEM when the electron beam hits a material such as silica, the sample can be affected. Other groups have demonstrated deformation processes of silicon oxide nanostructures induced by an electron beam [18,19]. Bombardment of high purity silica with electron and ion beams often results in the reduction of surface stoichiometry and release of $O_2$ [19]. While the sample diameters measured cannot be directly compared across techniques, silica was found to be deposited in both cases in the desired range of less than 5 nm, where it is sufficient to encapsulate and protect the fluorophore and modify the iron oxide surface to enhance biocompatibility.

Dynamic light scattering was used to characterize particle zeta potential and hydrodynamic diameter in solution. Characterizing the particle surface properties of the SCION particles is necessary to understand and predict their properties under physiological conditions and also to optimize conjugation chemistry. Hydrodynamic diameter and zeta potential relate when examining flocculation and colloidal stability. When the zeta potential is low ($-30\text{mV} < \zeta < 30\text{mV}$), electrostatic repulsion is no longer strong enough to prevent the particles from aggregating and the recorded hydrodynamic diameter reading also increases. SCION point of zero charge (PZC) was found to be at pH 2.5 (figure 4b). In the pH range where the zeta potential was low, the hydrodynamic diameter was higher, with its peak near the PZC. In the range above pH 5, a strong negative zeta potential (figure 4b) allowed the particles to remain in colloidal suspension with a diameter of ~18 nm (figure 4a). This hydrodynamic diameter was close to the TEM measurements of ~16–17 nm. Coating with silica made the agent anionic across the working pH range, as compared to uncoated USPIO which has a PZC at pH 7 [20]. SCION's stable negative charge in the pH range of 6–7 is desirable because it imitates the negative charge of most biomolecules [21]. Ideal for biomedical applications, the nanoparticles remain stable as a colloid without flocculation in the physiological pH range.

### 3.4. SCION Magnetic Hysteresis

To characterize particle behavior and to confirm that the particles were in fact superparamagnetic, hysteresis curves were analyzed. Magnetic domains of ferromagnetic materials have a magnetic memory where once aligned in an applied field, they do not return to their original state without expenditure of energy. This dependency on recent history traces a hysteresis loop and energy loss is measured by the area of the loop. Superparamagnetic materials have no permanent magnetic moment and, hence, no hysteresis loop. At 310 K, the shape of the hysteresis curves under both applied fields were tight with no hysteresis losses (figure 5), as is characteristic of a superparamagnet.

### 3.5. Examination of Fluorescence and Cell Viability

As demonstrated in its emissions spectrum (figure 6a), SCION particle was clearly excited by 635 nm excitation and would be able to be detected with the same excitation in flow cytometry. While it is always possible to know the molar equivalence of dye being reacted to particle, precisely quantifying the amount that attached is a true challenge. Typically, dye content is analyzed by fluorescence which is characterized by quantum yield. The method

for measuring quantum yield involves comparing the test sample to well characterized standard samples [22]. The ratio of the two samples' integrated fluorescence intensities recorded under identical conditions yield the ratio of the quantum yield values. This technique requires the assumption that the solvents of the two samples behave similarly. In the case of SCION particles, the assumption is not reasonable. The ideal standard to use here would be Cy5.5 in solution but the dye is not a reliable control given its low quantum yield of 0.23 [23]. Regardless of the standard chosen, the solvent properties of the two samples would also not be compatible given that iron oxide particles have an absorbance spectrum [16]. Also, accounting for the refractive index of the particles is difficult. Elemental analysis of the particle to measure sulfur content from the dye was attempted, however it was below reliable detection limits and the results were invalid. While we are continuing efforts to determine the number of active dyes per particle, because emissions are detectable, flow cytometry was used for *in vitro* analysis.

Monocyte, T-, and B-cell viability after incubation with SCION was observed by flow cytometry detection of particle fluorescence and amine-reactive viability dye. It is important to note that while the concentration of SCION particle used in all flow studies (0.05 nmol SCION/mL = 0.82 mM Fe) was chosen because of high staining of all cell populations after a 1 h incubation, it is significantly higher than would be used in a clinical setting. The injected dose for Feridex in healthy adults is 0.56 mg/kg [24], which for an average human weighing 70 kg and a blood volume of 4.7 L [25] equates to 0.15 mM Fe upon injection. *In vivo*, iron oxides are immediately challenged by the reticuloendothelial system (RES) and rapidly cleared from circulation, and therefore the injected concentration is not maintained. Thus, the viability studies have been conducted at a greater and sustained concentration that would not typically be observed clinically. Yet, after a 1 h incubation there was no significant effect on any cell population's viability (figure 6b). While monocytes retained particle, T- and B-lymphocytes did not past 24 h (figure 6c). It is well documented in the literature that macrophages have a propensity towards iron oxide particles. Monocytes are the precursors to macrophages, and it was expected that they would have higher SCION uptake than lymphocytes. Indeed, dextran-coated iron oxide has been shown to induce differentiation of monocytes into macrophages [26]. Some literature indicates that *in vitro*, fetal calf serum contributes to particle uptake particularly by macrophages with the explanation that opsonins coat particle surface and promote the adsorption and internalization of nanoparticles by specific receptors present on the macrophage membrane [27].

The results of longer incubation times with SCION also did not affect lymphocyte viability. Tsouchnikas and co-workers [28] evaluated the effect of iron load on peripheral blood lymphocytes and on circulating cytokine levels in iron-depleted hemodialysis patients receiving recombinant erythropoietin. They similarly determined no change in major lymphocyte subsets [28]. A decrease in monocyte viability was observed with longer incubation times at this sustained high concentration though viable cells also retained particle (figure 6d–e). Though here the method of particle uptake by monocytes was not studied, multiple mechanisms of internalization of magnetic nanoparticles have been reported, including phagocytosis, scavenger receptor-mediated endocytosis, fluid-phase endocytosis and diffusion [29]. Because of their smaller diameter, ultrasmall nanoparticles can escape phagocytosis and incorporate within cells [30]. This allows for interference with mitochondrial energy production and activation of proinflammatory signaling, oxidative stress by reactive oxygen species generation, or even apoptosis, particularly in cultured cells [26,29–34]. *In vivo*, macrophage suicide approaches with nanoparticles have been translated into therapeutic applications for macrophage-driven diseases such as bacterial infection, atherosclerosis, rheumatoid arthritis, neuroinflammation, blood disorders, and diabetes [35,36]. Comparatively, of a number of nanoparticles tested, iron oxide agents have been

shown to be the safest [37] and *in vivo* toxicity data demonstrates no long-term implications when administered at clinically relevant concentrations [26].

### 3.7. Animal Studies

Following i.v. injection, SCION particle accumulated in leaky tumor by EPR effect and then cleared within 24 h post-injection (Figure 7). These results demonstrate potential for *in vivo* diagnostic applications. If the agent is further conjugated to targeting ligands, there is opportunity for accumulation in leaky tumors, clearance of nonspecific uptake, and imaging with minimal background at times such as 24 h post-injection.

## 4. Conclusions

We have reported the engineering of a SCION particle that has both magnetic and optical properties. The particle design with silica as a buffering encapsulation of USPIO and Cy5.5 allows for strong contrast in both imaging modalities at no expense of one over the other. The 17–18 nm SCION is stable, biocompatible and targetable - all properties desirable for biomedical application.

The new frontier in medicine is treatment at the cellular level. By attaching a targeting ligand to this nanoparticle, it could be possible to better diagnose early-stage cancer, track stem cells, detect pathogens, and track the delivery of therapeutics by simultaneously gathering information using two distinct reporters. Targeting these particles with biomolecules such as antibodies creates a noninvasive reporting tool that can be used to monitor a variety of specific biological responses while providing valuable information regarding physiology and pathophysiology. As currently developed, the nanoparticle has many applications for detection and diagnostics both in the lab and the clinic. In addition, it can also be developed into a method of targeted drug delivery. Once the delivery particle is traced to its target location, the superparamagnetic properties of the USPIOs can then be exploited to heat, rupture and release a therapeutic drug payload. Superparamagnetic particles can also be used to locally heat and kill cancer cells. This technology has great potential to be a sensitive, minimally invasive, and highly specific method to trace biomolecules and deliver therapy.

## Supplementary Material

Refer to Web version on PubMed Central for supplementary material.

## Acknowledgments

We would like to thank Wei Lui and Yuxi Pang for providing the relaxation mapping tool. This research was supported by the Marshall Comission and the Intramural Research Program of the NIH, National Cancer Institute, Center for Cancer Research.

## REFERENCES

1. Coroiu I. Relaxivities of different superparamagnetic particles for application in NMR tomography. Journal of Magnetism and Magnetic Materials 1999;201:449–452.
2. Bumb A, Brechbiel MW, Choyke PL, Fugger L, Eggeman A, Prabhakaran D, Hutchinson J, Dobson PJ. Synthesis and characterization of ultra-small superparamagnetic iron oxide nanoparticles thinly coated with silica. Nanotechnology 2008;19:335601. [PubMed: 19701448]
3. Grosenick D, Wabnitz H, Rinneberg H, Moestra KT, Schlag PM. Development of a time-domain optical mammograph and first in vivo applications. App. Opt 1999;38:2927–3038.
4. Weissleder R. A clearer vision for in vivo imaging. Nat. Biotech 2001;19:316–317.

5. Andersson-Engels S, Wilson BC. In vivo fluorescence in clinical oncology: fundamental and practical issues. J. Cell Pharmacol 1992;3:48–60.
6. Wagnières GA, Star WM, Wilson BC. In Vivo Fluorescence Spectroscopy and Imaging for Oncological Applications. Photochem. Photobiol 1998;68:603–632. [PubMed: 9825692]
7. Mujumdar SR, Mujumdar RB, Grant CM, Waggoner AS. Cyanine-Labeling Reagents:  Sulfobenzindocyanine Succinimidyl Esters. Bioconj. Chem 1996;7:356–362.
8. Mulvaney P, Liz-Marzan LM, Giersig M, Ung T. Silica encapsulation of quantum dots and metal clusters. J.Mater.Chem 2000;10:1259–1270.
9. Liu DM, Chen IW. Encapsulation of protein molecules in transparent porous silica matrices via an aqueous colloidal sol-gel process. Acta Materialia 1999;47:4535–4544.
10. Santra S, Zhang P, Wang KM, Tapec R, Tan WH. Conjugation of biomolecules with luminophore-doped silica nanoparticles for photostable biomarkers. Analytical Chemistry 2001;73:4988–4993. [PubMed: 11681477]
11. Swadeshmukul S, Kemin W, Rovelyn T, Weihong T. Development of novel dye-doped silica nanoparticles for biomarker application. J Biomedical Optics 2001;6:160–166.
12. Xue Z, Liang D, Li Y, Long Z, Pan Q, Liu X, Wu L, Zhu S, Cai F, Dai H, Tang B, Xia J. Silica nanoparticle is a possible safe carrier for gene therapy. Chin. Sci. Bull 2005;20:2323–2327.
13. Jin Y, Kannan S, Wu M, Zhao JX. Toxicity of Luminescent Silica Nanoparticles to Living Cells. Chem. Res. Toxicol 2007;20:1126–1133. [PubMed: 17630705]
14. Ulman A. Formation and Structure of Self-Assembled Monolayers. Chem.Rev 1996;96:1533–1554. [PubMed: 11848802]
15. Bardosova M, Tredgold RH. Ordered layers of monodispersive colloids. Journal of Materials Chemistry 2002;12:2835–2842.
16. Ziolo RF, Giannelis EP, Weinstein BA, Ohoro MP, Ganguly BN, Mehrotra V, Russell MW, Huffman DR. Matrix-Mediated Synthesis of Nanocrystalline Gamma-Fe2o3 - a New Optically Transparent Magnetic Material. Science 1992;257:219–223. [PubMed: 17794752]
17. O'Grady K, Bradbury A. Particle Size Analysis in Ferrofluids. J Magn Magn Mater 1983;39:91.
18. Storm AJ, Chen JH, Ling XS, Zandbergen HW, Dekker C. Electron-beam-induced deformations of SiO[sub 2] nanostructures. Journal of Applied Physics 2005;98:014307–014308.
19. Pitts JR, Czanderna AW. Reduction of Silica Surfaces with Particle Beams. Nuclear Instruments and Methods in Physics Research 1986;B13:245–249.
20. Gomez-Lopera SA, Plaza RC, Delgado AV. Synthesis and characterization of spherical magnetite/biodegradable polymer composite particles. Journal of Colloid and Interface Science 2001;240:40–47. [PubMed: 11446784]
21. Vroman L. Surface Charge, Protein Adsorption, and Thrombosis. Science 1974;184:585–586. [PubMed: 4821961]
22. Williams ATR, Winfield SA, Miller JN. Relative fluorescence quantum yields using a computer controlled luminescence spectrometer. Analyst 1983;108:1067.
23. Mujumdar SR, Mujumdar RB, C.M G, Waggoner AS. Cyanine-labeling reagents: sulfobenzindocyanine succinimidyl esters. Bioconj. Chem 1996;7:356–362.
24. Feridex, IV. homepage on the Internet. Wayne, NJ: Bayer HealthCare Pharmaceuticals; [cited 2009 September 30]. updated 2007 May, Available from: http://berlex.bayerhealthcare.com/html/products/pi/Feridex_PI.pdf?WT.mc_id=www.berlex.com
25. World Book Rush-Presbyterian-St. Lukes Medical Center Medical Encyclopedia. Chicago: World Book; 1995. p. 120-121.
26. Shubayev VI, Pisanic Ii TR, Jin S. Magnetic nanoparticles for theragnostics. Adv. Drug Delivery Rev 2009;61:467–477.
27. Henry-Toulmé N, Grouselle M, Ramaseilles C. Multidrug resistance bypass in cells exposed to doxorubicin-loaded nanospheres : Absence of endocytosis. Biochem. Pharmacol 1995;50:1135–1139. [PubMed: 7488226]
28. Tsouchnikas I, Tsilipakou M, Daniilidis M, Kyriazis G, Pasadakis P, Parapanissiou E, Vargemezis V, Tsakiris D. Effect of Iron Loading on Peripheral Blood Lymphocyte Subsets and on Circulating

Cytokine Levels in Iron-Depleted Hemodialysis Patients Receiving Erythropoietin. Neph. Clin. Prac 2007;107:c97–c102.

29. Unfried K, Albrecht C, Klotz L-O, Von Mikecz A, Grether-Beck S, Schins RPF. Cellular responses to nanoparticles: Target structures and mechanisms. Nanotoxicology 2007;1:52–71.
30. Oberdorster G, Oberdorster E, Oberdorster J. Nanotoxicology: an emerging discipline evolving from studies of ultrafine particles. Environ. Health Perspect 2005;113:823–839. [PubMed: 16002369]
31. Nel A, Xia T, Madler L, Li N. Toxic Potential of Materials at the Nanolevel. Science 2006;311:622–627. [PubMed: 16456071]
32. Oberdörster G, Stone V, Donaldson K. Toxicology of nanoparticles: A historical perspective. Nanotoxicology 2007;1:2–25.
33. Monteiller C, Tran L, MacNee W, Faux S, Jones A, Miller B, Donaldson K. The pro-inflammatory effects of low-toxicity low-solubility particles, nanoparticles and fine particles, on epithelial cells in vitro: the role of surface area. Occup. Environ. Med 2007;64:609–615. [PubMed: 17409182]
34. Naveau A, Smirnov P, Ménager C, Gazeau F, Clément O, Lafont A, Gogly B. Phenotypic Study of Human Gingival Fibroblasts Labeled With Superparamagnetic Anionic Nanoparticles. J. Periodontol 2006;77:238–247. [PubMed: 16460250]
35. Chellat F, Merhi Y, Moreau A, Yahia LH. Therapeutic potential of nanoparticulate systems for macrophage targeting. Biomaterials 2005;26:7260–7275. [PubMed: 16023200]
36. Vega-Villa KR, Takemoto JK, Yáñez JA, Remsberg CM, Forrest ML, Davies NM. Clinical toxicities of nanocarrier systems. Adv. Drug Delivery Rev 2008;60:929–938.
37. Gojova A, Guo B, Kota RS, Rutledge JC, Kennedy IM, Barakat AI. Induction of inflammation in vascular endothelial cells by metal oxide nanoparticles: Effect of particle composition. Environ. Health Perspect 2007;115:403–409. [PubMed: 17431490]

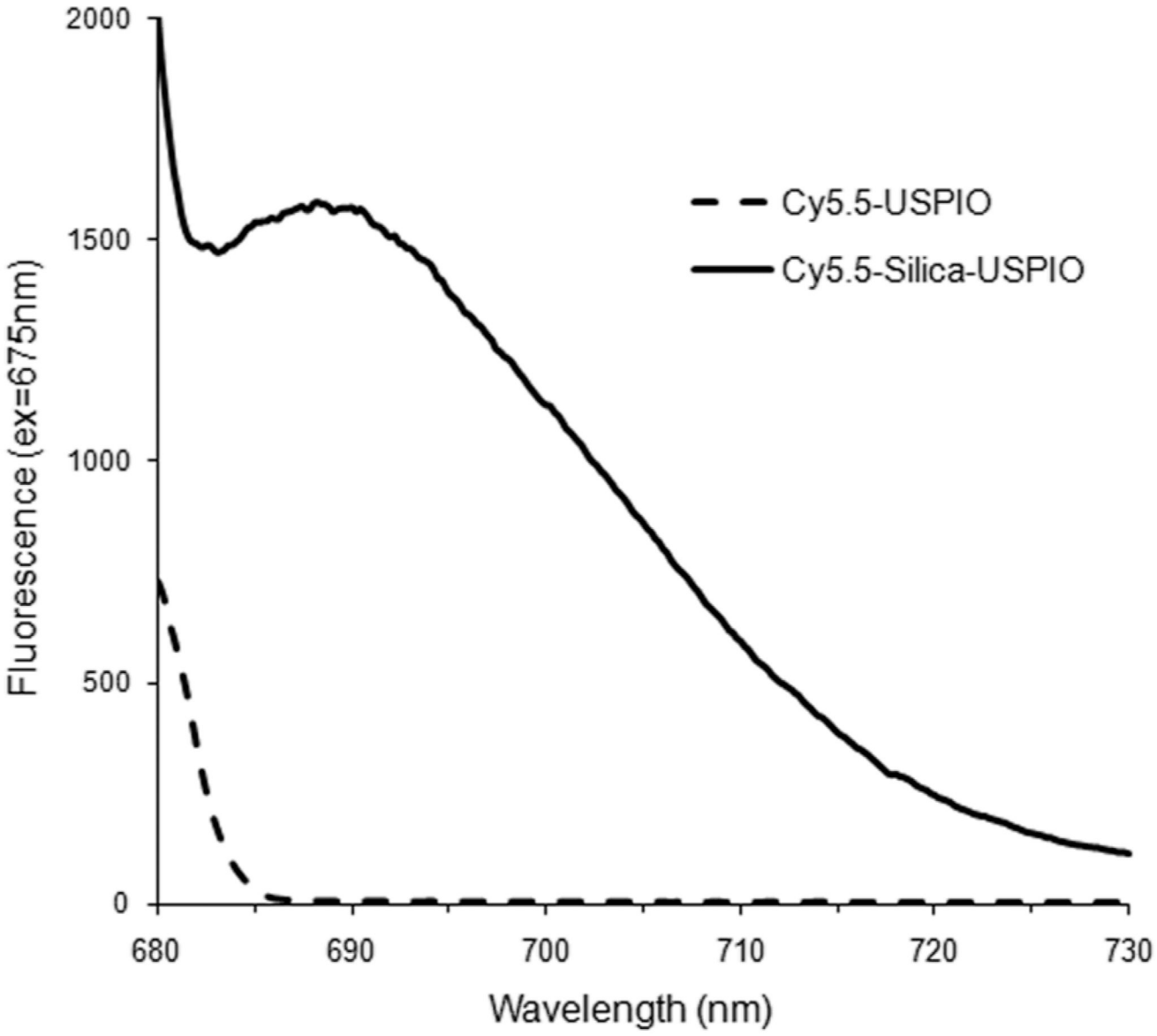


**Figure 1.**
Emissions spectrum of Cy5.5 conjugated either directly to USPIO or to silica-coated USPIO

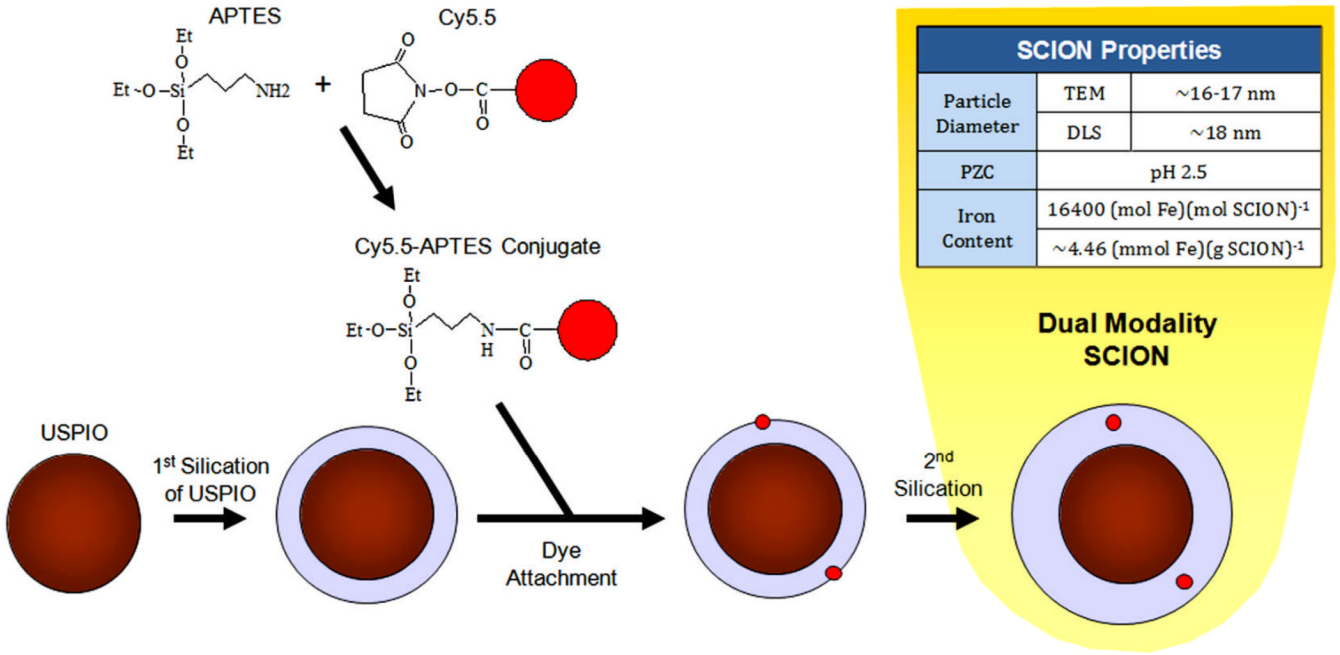


**Figure 2.**
SCION particle synthesis.

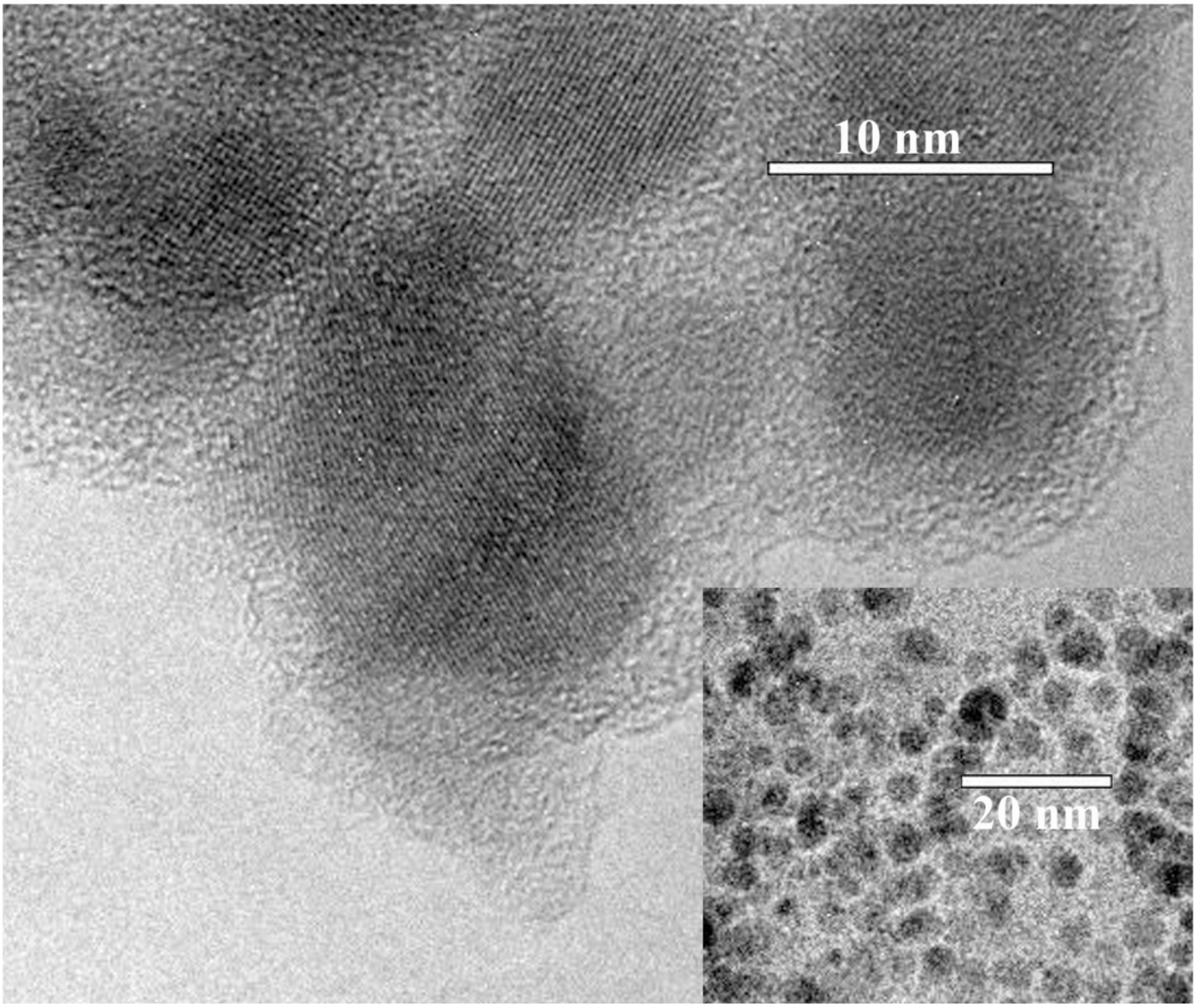


**Figure 3.**
Transmission electron microscopy of synthesized SCION particles.

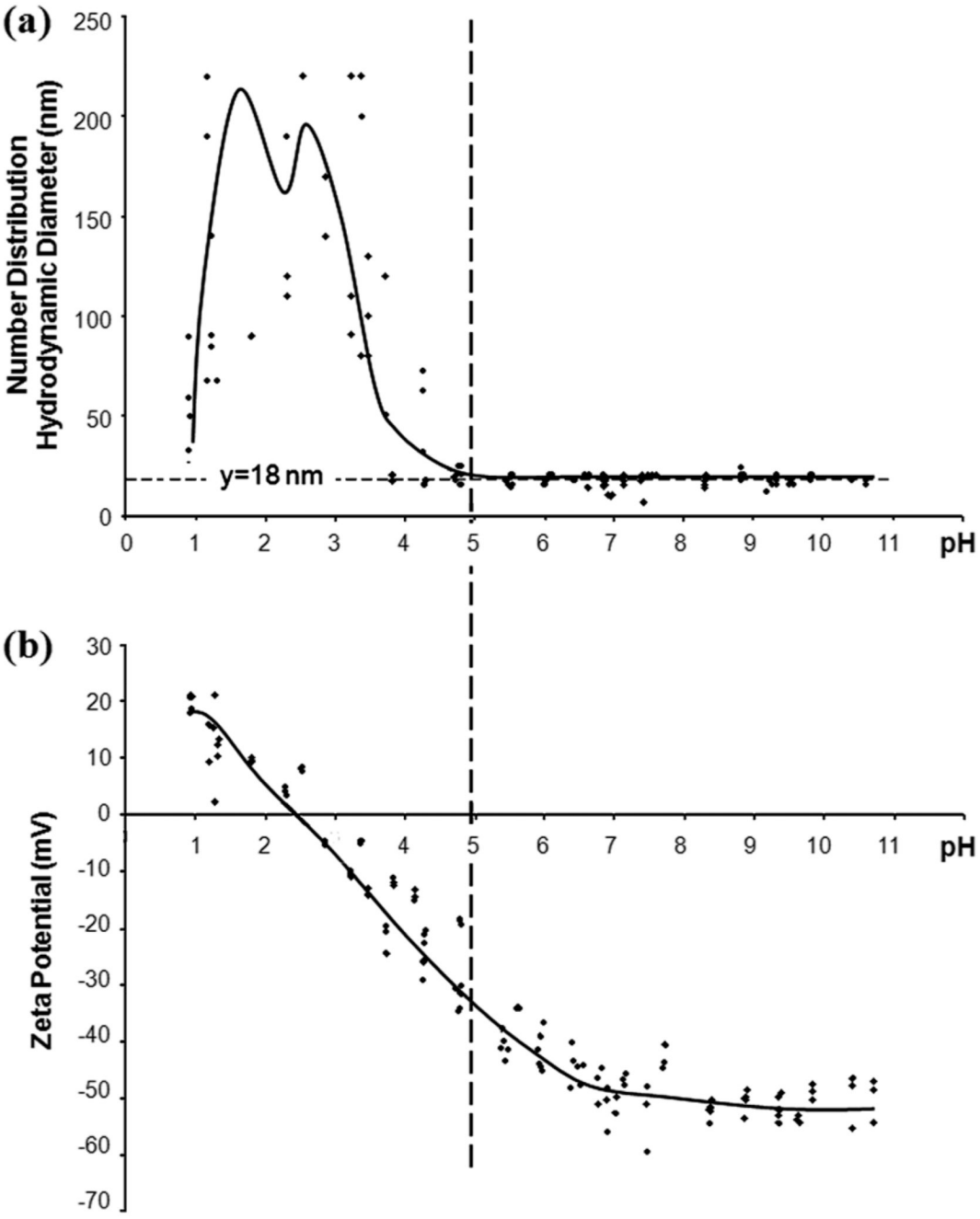


**Figure 4.**

SCION particles characterized across pH range for (a) number distribution hydrodynamic diameter and (b) zeta potential. At >pH 5, the absolute value of the zeta potential was less than 30 mV and flocculation was observed. Right of the dotted line, zeta potential was strong and the observed hydrodynamic diameter was ~18 nm.

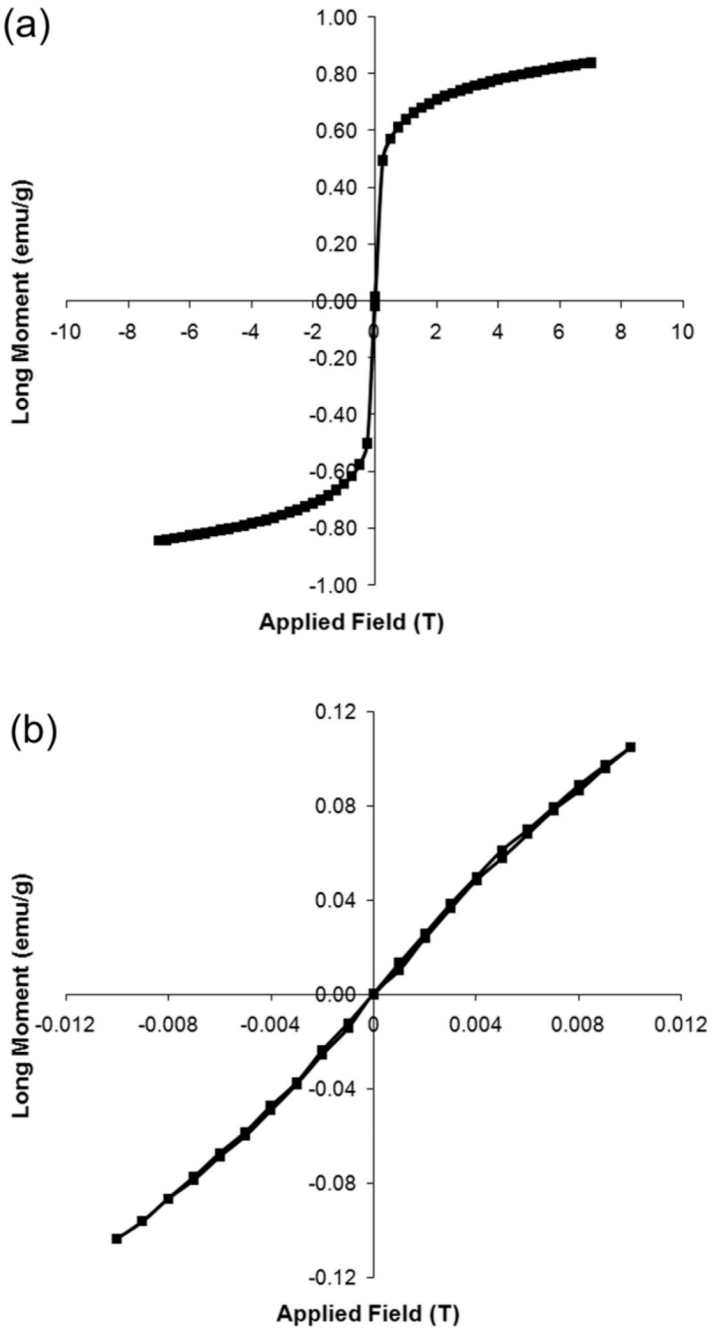


**Figure 5.**
SCION magnetic hysteresis results at 310K and (a) ±7 T and (b) ±0.01 T, demonstrating superparamagnetic behavior.

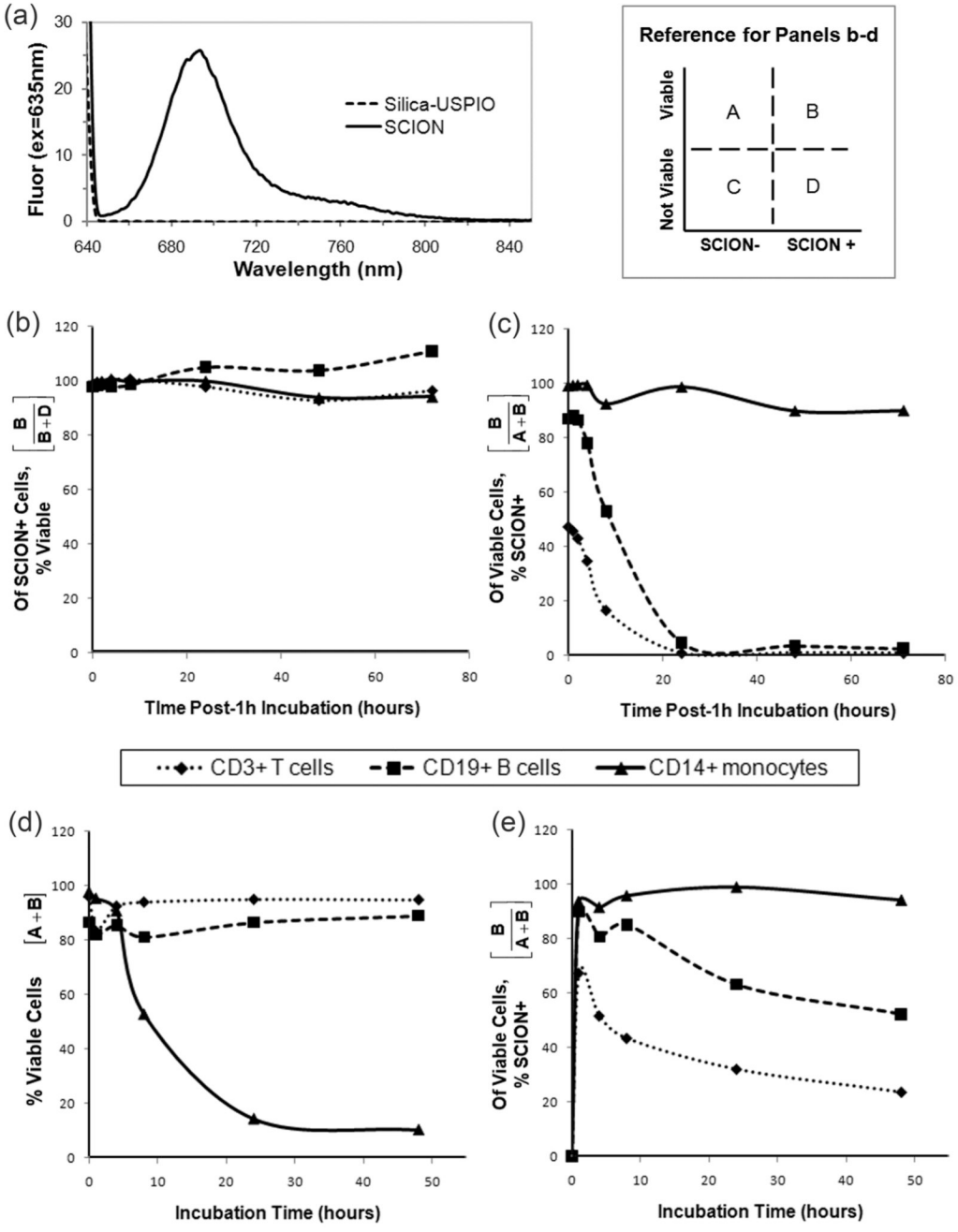


**Figure 6.**

Particle fluorescence and T-cell, B-cell, and monocyte viability analysis. (a) Fluorescence spectrum of SCION and unlabeled USPIO with excitation at 635nm. *Study 1: Evaluation post 1hr-incubation with SCION* (b) the percentage of SCION-stained cells that are viable (normalized to control) and (c) the percentage of viable cells that are SCION-stained. *Study 2: After various incubation times with SCION*, (d) the total percentage of viable cells and (e) the percentage of viable cells that are SCION-stained.

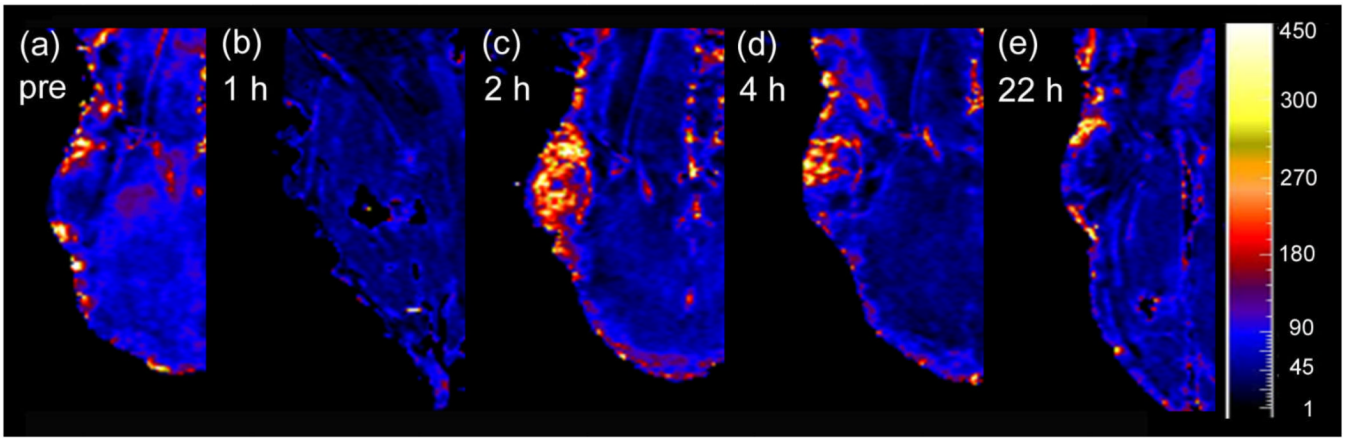


**Figure 7.**

*In vivo* application of SCION particle for EPR effect into leaky tumors. $R_2$ maps of a A431-tumor bearing mouse at (a) pre-injection, (b) 1 h, (c) 2 h, (d) 4 h, and (e) 22 h post-i.v. injection demonstrates peak particle retention at 2 h post-injection.